Supporting Information

Strong Second-Harmonic Generation and Wide Temperature Range Switching Behavior Coexisting in An Ultrawide-Bandgap Selenate

Yang Chi, Mei-Ling Xin*

School of Chemistry and Chemical Engineering, Qufu Normal University, Qufu 273165, P. R. China

Corresponding author: yang.chi@hotmail.com

Synthesis

The reactants were used as received without further purification. Rb_2CO_3 (0.462 g, 99.8%) was dissolved in H_2SeO_4 (1.450 g, 40%), then evaporated at room temperature and finally colorless block RHSO crystals were obtained in about 95% yield (based on Rb).

Single crystal X-ray diffraction

Single-crystal X-ray diffraction measurements were performed on a Bruker D8 QUEST X-ray diffractometer equipped with graphite-monochromated Mo Kα (λ = 0.71073 Å) radiation at 300, 360 and 388 K (CSD 2424193–2424195). Within *OLEX*^{2},[1] the structures were solved by intrinsic phasing method with *SHELXT*[2]and refined by full-matrix least squares techniques on F^2 with anisotropic thermal parameters for all atoms with *SHELXL* (Sheldrick, 2015)[3]. The crystallographic data describe by conventional and non-conventional lattices, atomic coordinates, and important bond lengths are summarized in **Tables S1**−**S4**, respectively.

Powder X-ray diffraction

The purity of as-prepared was confirmed using a powder X-ray diffraction (PXRD) technique (**Figure S1**). The PXRD pattern was measured using a PANalytical X'Pert^3 diffractometer for Cu Kα radiation (λ = 1.5406 Å) at room temperature. The simulated patterns were produced using the Mercury v2.1 program provided by the Cambridge Crystallographic Data Center and single-crystal reflection data.

Thermal analysis

Thermal stability was evaluated using a DZ-STD300 TGA/DSC thermal analyzer instrument under the flow of N_2 in the temperature range 22−800 °C at a heating rate of 10 °C/min. DSC measurements were carried out on a DSC thermal analyzer instrument (DZ-DSC300C, Nanjing, China) under the flow of N_2 at a heating/ cooling rate of 10℃/min.

UV-vis-NIR diffuse reflectance spectroscopy

The diffuse reflectance spectrum was recorded at room temperature on a computer-controlled Shimadzu UV-3600 spectrometer equipped with an integrating sphere in the wavelength range of 180–2500 nm.

UV transmission spectroscopy

The variable-temperature transmission spectrum was recorded on a computer-controlled Metash UV-8000A spectrometer in the wavelength range of 190–1000 nm.

SHG Measurements

SHG measurement on powder crystalline sample of RHSO was performed with a modified Kurtz-Perry powder method[4] using a Q-switched Nd:YAG laser at 1064 nm wavelength.

Theoretical Calculation

Computation details of LTP. Electronic structure calculation of RHSO were carried out within the framework of density functional theory (DFT) by using the *CASTEP* package[5]. The generalized gradient approximation (GGA) within the Perdew−Burke−Ernzerhof (PBE)-type exchange-correlation potentials were used[6]. The employed OTFG norm-conserving pseudopotentials of Rb, H, Se, and O treat 4s 4p 5s, 1s, 3d 4s 4p, and 2s 2p as the valence states, respectively. The plane-wave cutoff energy of 1350 eV and the threshold of 5×10^{-7} eV/atom were set for the self-consistent-field convergence of the total electronic energy. A 6 × 4 × 3 Monkhorst-Pack k-point grid in the Brillouin Zone of the primitive cell is chosen and more than 230 empty bands were involved in the calculations to ensure the convergence of SHG coefficients. Scissors implementation within length-gauge formulations of the frequency dependent NLO response equations used to calculate the second-order response function were originally derived by Aversa and Sipe and later modified by F. Nastos et al[7,8].

Band gap evaluation of LTP by hybrid functional calculation. One of the requirements for a deep-ultraviolet NLO material is an exceptionally wide bandgap. Consequently, precise determination of bandgap plays a crucial role in material design and property prediction. While planewave DFT demonstrates excellent capability in predicting optical characteristics such as birefringence and SHG coefficients,[9] its application with the GGA as the exchange-correlation functional typically results in significant underestimation of bandgap values.[10] Therefore, to obtain bandgap values closer to experimental measurements, the bandgap of LTP was calculated using the Heyd−Scuseria−Ernzerhof (HSE06) hybrid functional based on a screened Coulomb potential[11,12] while other parameters were kept unchanged. A calculated result of 6.34 eV was obtained (**Figure S2**), which shows good agreement with the experimental value of 6.56 eV.

Computation details of HTP. The DFT and *ab initio* molecular dynamics (AIMD) calculations were carried out using the *CASTEP* package[5]. The GGA of PBE was

selected as the electronic exchange–correlation potential[6].

Based on the experimentally determined structure at 388 K, a 1 × 2 × 2 supercell (containing 168 atoms) was constructed for AIMD calculations. AIMD was carried out under NVT ensemble[13]. Grimme's DFT-D2[14] dispersion corrections were incorporated in the computations. The total simulation time was set to 2000 fs with time step of 1 fs. The Nose–Hoover chain thermostat[15] was used to control the temperature at 388 K. The first Brillouin zone was sampled at the Γ point, only. Ultrasoft pseudopotential was used to describe the interaction between ionic and the valence electron in all calculations[16]. The cutoff energy and the convergence criterion were set to 340 eV and 10^{-5} eV, respectively.

In the obtained dynamical sublattice, 20 structures were randomly selected as representatives, and their optical properties were calculated. A 1 × 3 × 6 Monkhorst-Pack k-point grid in the Brillouin Zone of the primitive cell is chosen and more than 450 empty bands were involved in the calculations to ensure the convergence of SHG coefficients. The remaining computational details are entirely identical to those of LTP.

Table S1. Crystal data and structure refinement parameters for RHSO describe by conventional lattices.

	RHSO-LTP	**RHSO-"ITP"**	**RHSO-HTP**
***T* (*K*)**	300	360	388
cryst syst	triclinic		monoclinic
space group	*P*1		*C*2
Z	3		6
***a* (Å)**	4.6181(3)	4.6245(2)	19.9401(11)
***b* (Å)**	7.5724(5)	7.5938(4)	7.6068(4)
***c* (Å)**	10.6170(7)	10.6496(7)	4.6292(2)
***α* (°)**	69.154(2)	69.145(2)	90
***β* (°)**	77.963(2)	78.003(2)	102.751(3)

γ (°)	89.597(2)	89.743(2)	90
V (Å^3)	338.43(4)	340.86(3)	684.84(6)
D_{calcd} (g/cm^3)	3.377	3.353	3.338
μ (mm^{-1})	18.917	18.782	18.697
F(000)	312.0	312.0	624.0
2θ range (°)	4.208–64.802	4.196–64.634	4.188–64.706
measd reflns	13470	13578	13700
indep reflns/R_{int}	3756/0.0442	3763/0.0459	2116/0.0501
obsd reflns	3401	3227	1841
R_1, wR_2 ($I > 2\sigma(I)$)[a]	0.0342, 0.0776	0.0330, 0.0713	0.0290, 0.0619
R_1, wR_2 (all data)[a]	0.0400, 0.0799	0.0426, 0.0742	0.0384, 0.0646
GOF on F^2	1.033	0.989	1.035
Flack parameter	−0.024(12)	−0.015(13)	−0.011(13)
$\Delta\rho_{max}/\Delta\rho_{min}$, e/Å^3	0.91/−1.42	0.80/−1.06	0.71/−0.80

[a] $R_1 = \Sigma||F_o| - |F_c||/\Sigma|F_o|$; $wR_2 = \{\Sigma[w(F_o^2 - F_c^2)^2]/\Sigma[w(F_o^2)^2]\}^{1/2}$.

Table S2. Crystal data for RHSO describe by non-conventional lattices.

	RHSO-LTP	RHSO-"ITP"	RHSO-HTP
T (K)	300	360	388
cryst syst	triclinic		monoclinic
space group	$I1$		$I2$
Z	6		
a (Å)	4.6181(3)	4.6245(2)	4.6292(2)
b (Å)	7.5724(5)	7.5938(4)	7.6068(4)
c (Å)	19.3573(13)	19.4143(13)	19.4497(10)
α (°)	89.856(3)	89.906(3)	90
β (°)	90.720(3)	90.683(3)	90.672(2)

***γ* (°)**	90.403(2)	90.257(2)	90
***V* (Å³)**	676.85(8)	681.73(7)	684.84(6)

Table S3. Fractional atomic coordinates (×10⁴) and equivalent isotropic displacement parameters (U_{eq}[a], Å² × 10³) for RHSO-LTP, -"ITP", and -HTP describe by non-conventional lattices. Site A and B are equivalent in the HTP.

		LTP		"ITP"		HTP
		site A	**site B**	**site A**	**site B**	
Rb1	***x***	−10008(2)		−10012(2)		−10000
	y	13349.1(12)		13349.8(12)		13342.1(14)
	z	4.1(5)		3.5(5)		0
	U_{eq}	28.1(2)		35.7(2)		39.1(2)
Rb2	***x***	−4176.4(19)	−10878.6(19)	−4189(2)	−10858.7(19)	−4172.6(14)
	y	9346.0(11)	4331.4(11)	9341.5(11)	4333.7(11)	9329.0(10)
	z	1657.3(5)	3349.1(5)	1657.9(5)	3347.4(5)	1655.5(3)
	U_{eq}	28.0(2)	28.6(2)	35.5(2)	35.6(2)	38.67(18)
Se1	***x***	−9966.2(19)		−9987.6(18)		−10000
	y	8473.5(11)		8477.1(10)		8470.3(11)
	z	−4.4(4)		−2.0(4)		0
	U_{eq}	18.88(18)		23.96(18)		26.2(2)
Se2	***x***	−5359.5(14)	283.2(14)	−5342.6(14)	281.1(14)	−5309.4(10)
	y	4244.0(9)	9240.1(9)	4242.1(9)	9240.2(9)	4233.1(7)
	z	1677.1(4)	3329.5(4)	1676.4(4)	3329.2(4)	1673.8(3)
	U_{eq}	20.5(2)	20.6(2)	25.9(2)	25.5(2)	27.88(16)
O1	***x***	−12569(13)	−7437(13)	−12569(12)	−7447(12)	−12558(9)

	y	7103(8)	7159(8)	7122(8)	7150(8)	7124(7)
	z	297(3)	−294(3)	296(3)	−292(3)	290(2)
	U_{eq}	29.3(13)	27.4(12)	34.3(13)	34.2(13)	37.1(10)
O2	***x***	−7895(14)	2864(14)	−7886(13)	2851(14)	−7858(9)
	y	5618(9)	10618(9)	5613(8)	10616(9)	5606(7)
	z	1323(3)	3681(3)	1327(3)	3679(3)	1326(2)
	U_{eq}	30.3(13)	32.9(14)	37.6(14)	39.4(14)	43.8(11)
O3	***x***	−8870(15)	−11246(15)	−8866(14)	−11202(15)	−8828(10)
	y	9630(8)	9646(8)	9634(8)	9642(8)	9632(5)
	z	645(3)	−628(3)	642(3)	−629(3)	636(2)
	U_{eq}	32.3(15)	31.7(14)	41.3(16)	41.9(16)	43.8(12)
O4	***x***	−2803(13)	−2253(13)	−2797(12)	−2253(13)	−2772(8)
	y	5576(8)	10577(8)	5572(8)	10564(8)	5565(7)
	z	1948(3)	3062(3)	1945(3)	3062(4)	1936(2)
	U_{eq}	29.5(13)	31.2(14)	39.0(14)	39.4(15)	42.8(11)
O5	***x***	−6779(16)	1667(17)	−6752(16)	1659(16)	−6696(11)
	y	3167(10)	8187(9)	3168(10)	8184(10)	3170(8)
	z	2300(4)	2702(4)	2297(4)	2705(4)	2294(3)
	U_{eq}	39.5(17)	41.3(17)	51.1(18)	51.0(18)	57.0(14)
O6	***x***	−4334(16)	−741(17)	−4323(16)	−731(16)	−4303(12)
	y	3016(9)	7989(9)	3021(9)	8007(9)	3003(7)
	z	1046(3)	3957(4)	1050(3)	3959(4)	1047(3)
	U_{eq}	37.7(15)	39.4(16)	45.6(16)	47.6(17)	52.1(12)
H1	***x***	−14520(120)		−14490(130)		−14550(160)

	y	7300(140)		7270(150)		7370(170)
	z	50(50)		30(50)		90(50)
	U_{eq}	30(30)		50(30)		50(40)
H2	***x***	−9660(130)	4730(150)	−9580(130)	4710(140)	−9620(100)
	y	5810(130)	10950(160)	5800(120)	10830(160)	5800(130)
	z	1610(40)	3440(60)	1630(40)	3420(50)	1610(30)
	U_{eq}	30(30)	60(40)	30(30)	70(40)	60(20)

[a] U_{eq} is defined as one third of the trace of the orthogonalized U_{ij} tensor.

Table S4. Important interatomic distances (Å) for RHSO.

	LTP	**"ITP"**	**HTP**
Se1−O1(A)	1.691(6)	1.680(6)	1.669(5)
Se1−O1(B)	1.644(6)	1.656(6)	1.669(5)
Se1−O3(A)	1.608(6)	1.608(6)	1.610(4)
Se1−O3(B)	1.607(6)	1.601(6)	1.609(4)
Se2(A)−O2(A)	1.708(6)	1.708(6)	1.709(4)
Se2(B)−O2(B)	1.714(6)	1.714(6)	
Se2(A)−O4(A)	1.630(6)	1.629(6)	1.629(4)
Se2(B)−O4(B)	1.632(6)	1.627(6)	
Se2(A)−O5(A)	1.599(6)	1.598(6)	1.592(5)
Se2(B)−O5(B)	1.598(7)	1.595(7)	
Se2(A)−O6(A)	1.615(6)	1.607(6)	1.611(5)
Se2(B)−O6(B)	1.612(6)	1.612(6)	
O1(A)···O1(B)[1]	2.510(8)	2.516(8)	2.516(8)
O1(A)−H1	1.03(3)	1.03(3)	1.02(3)
O1(B)···H1	1.50(4)	1.50(4)	1.53(4)

H1···H1’	-	-	0.53(3)
O2(A)···O4(A)[1]	2.583(9)	2.581(9)	2.578(6)
O2(B)···O4(B)[2]	2.567(10)	2.575(9)	
O2(A)–H2(A)	1.01(3)	1.00(3)	1.00(3)
O2(B)–H2(B)	1.01(3)	1.01(3)	
O4(A)[1]···H2(A)	1.61(4)	1.62(4)	1.61(4)
O4(B)[2]···H2(B)	1.61(6)	1.59(5)	

[1]−1+*X*, +*Y*, +*Z* for LTP and “ITP” ; −3−*X*, +*Y*, −*Z* for HTP describe by non-conventional lattices

[2]1+*X*, +*Y*, +*Z* for LTP and “ITP” ; −1+*X*, +*Y*, +*Z* for HTP describe by non-conventional lattices

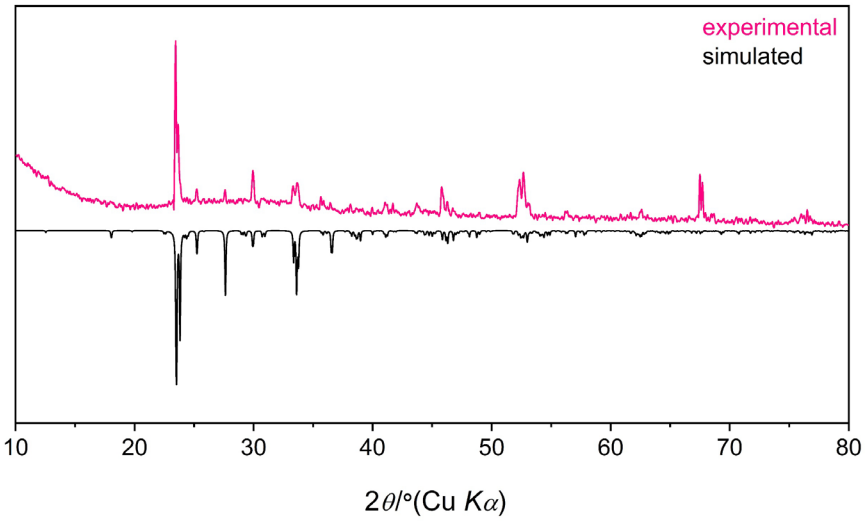

Figure S1. X-ray powder diffraction pattern of RHSO-LTP.

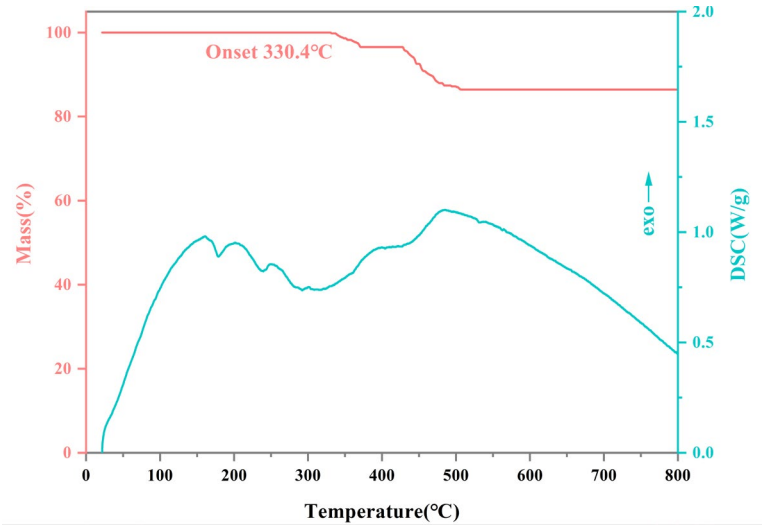

Figure S2. The TG-DSC curves of RHSO.

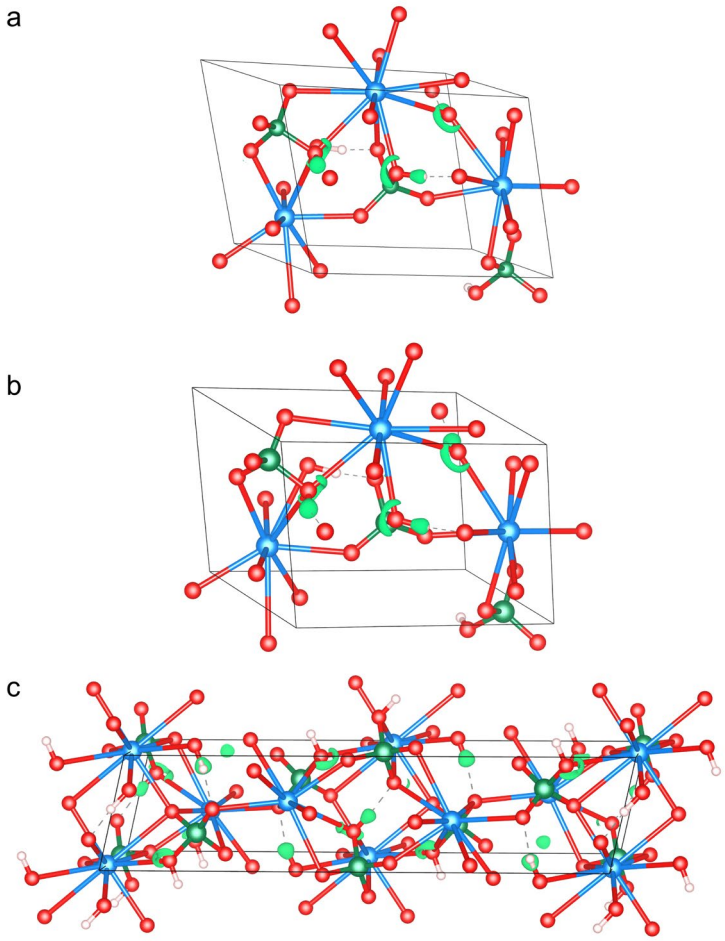

Figure S3. Crystal structure and calculated electron localization function isosurface maps of RHSO-LTP **a**), -"ITP" **b**), and -HTP **c**).

In simple terms, the transitions among the LTP, "ITP," and HTP originate from the hopping of the H1 atom. The specific differences are as follows: the H1 atom in the structure resides in a double-well potential with two equilibrium positions. In the LTP, H1 almost exclusively occupies one side of the potential well. In the higher-temperature "ITP," H1 begins to frequently hop to the opposite equilibrium position. With a further increase in temperature, the probability of the H1 atom occupying both wells in the HTP becomes equal, thereby inducing the formation of a new twofold axis in the structure (Figure 1b).

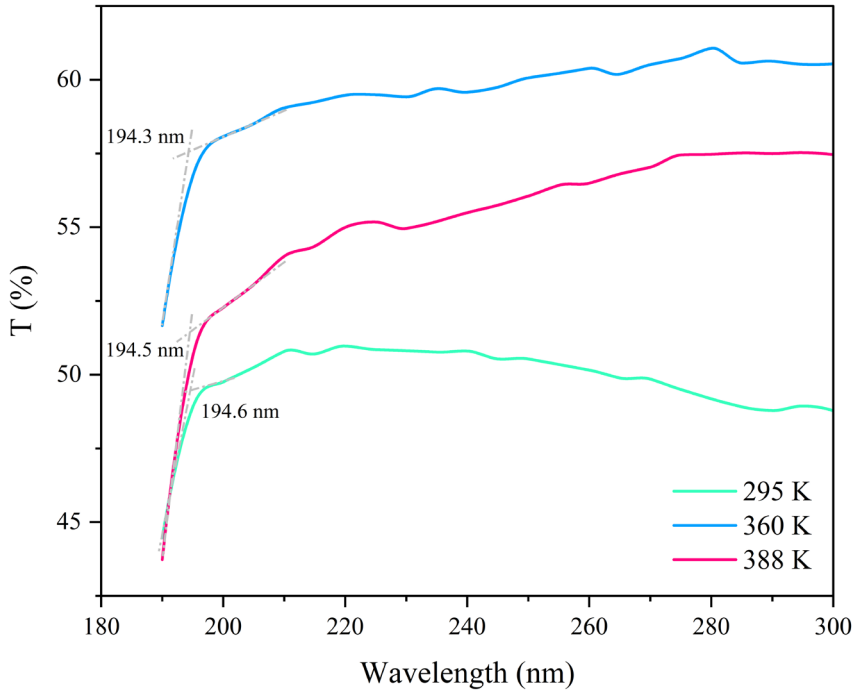

Figure S4. The variable-temperature transmission spectrum of RHSO.

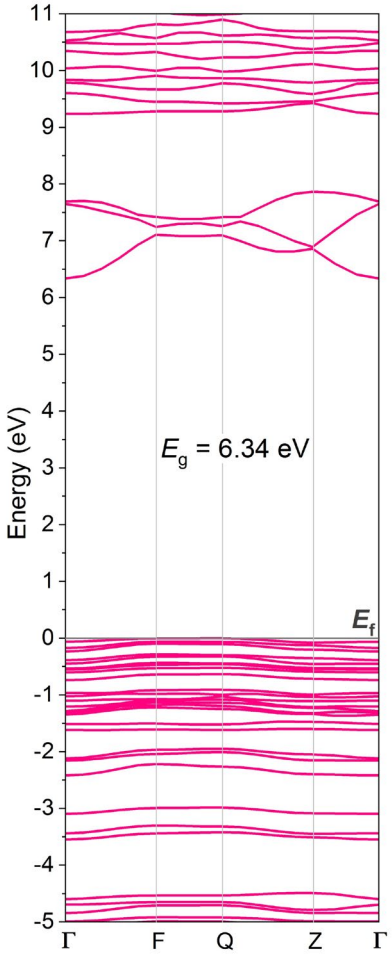

Figure S5. Calculated band structure for RHSO-LTP using the hybrid functional HSE06.

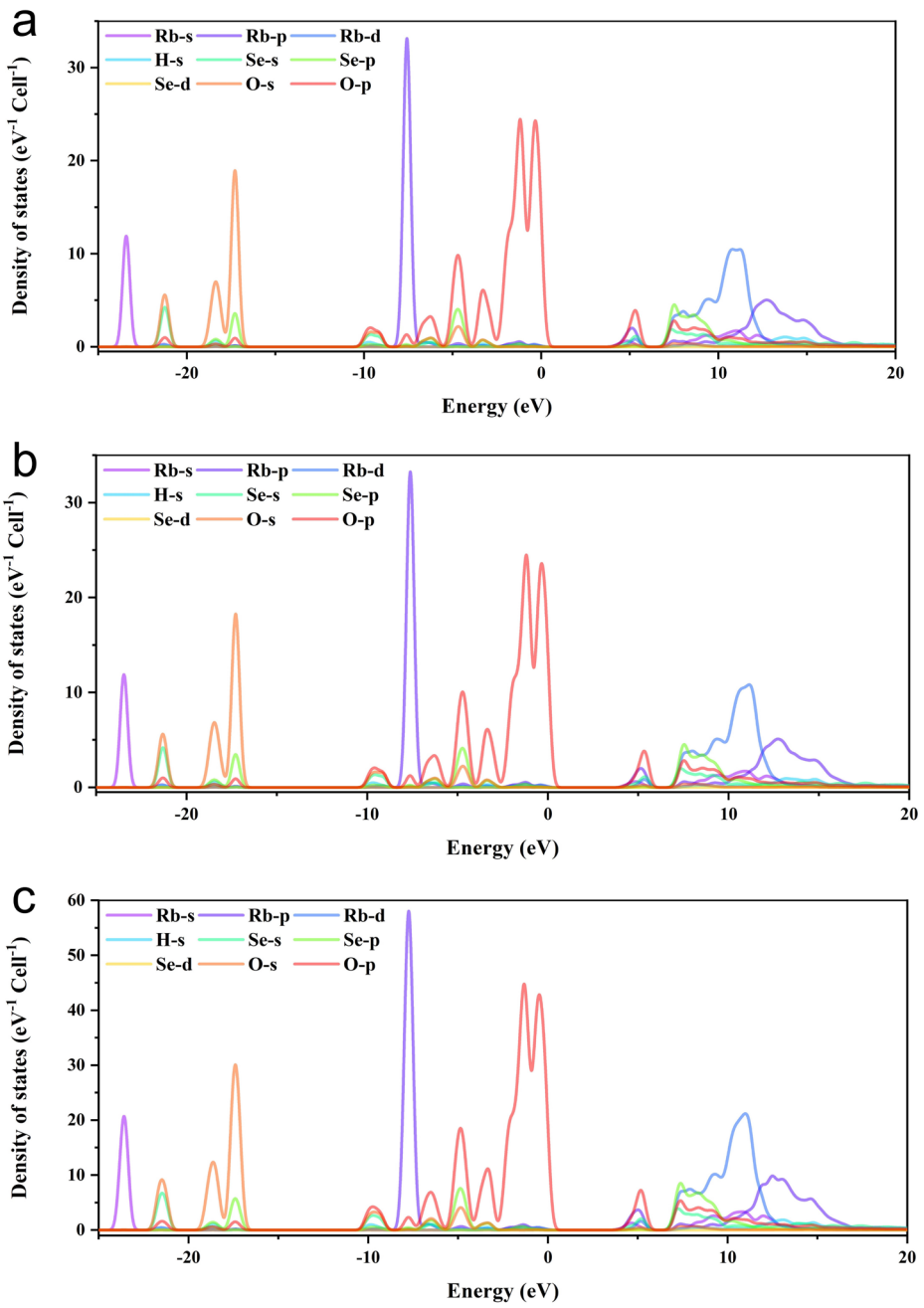

Figure S6. Calculated projected density of states for RHSO-LTP **a**), -"ITP" **b**), and -HTP **c**).

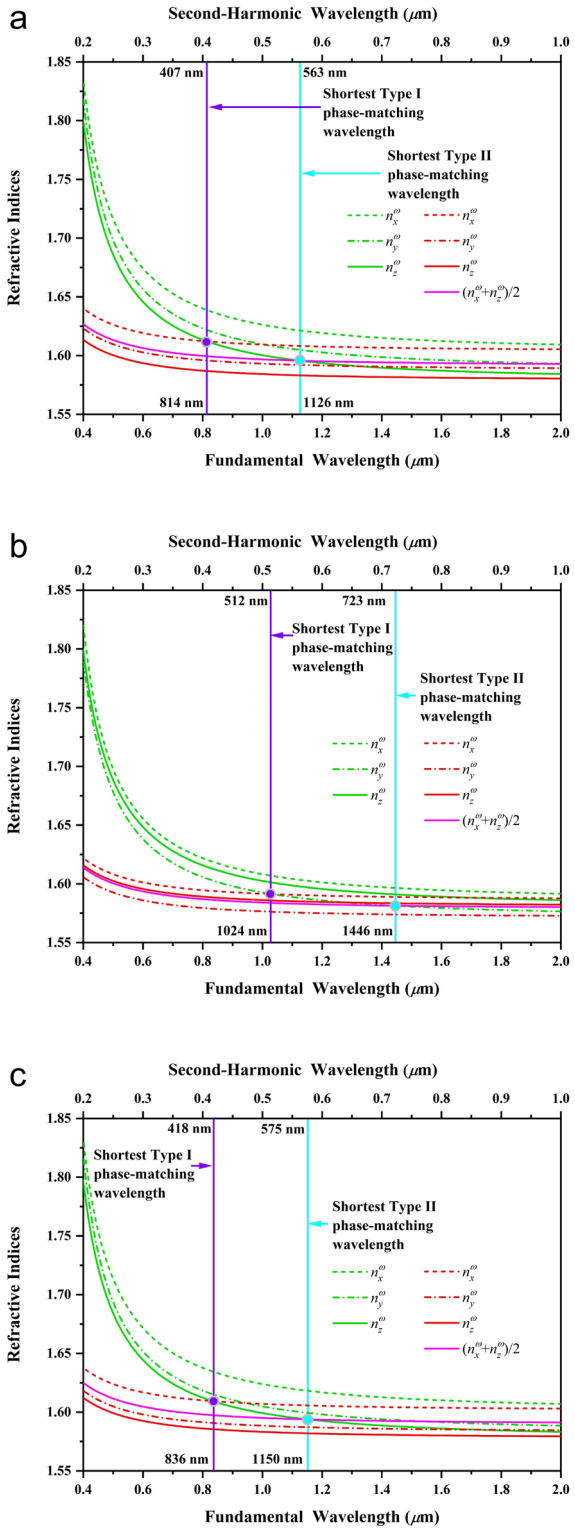

Figure S7. Calculated shortest phase-matching wavelength for RHSO-LTP **a**), -"ITP" **b**), and -HTP **c**).

One point to note is that theoretical calculations indicate that RHSO lacks sufficiently large birefringence to achieve phase matching in the deep ultraviolet spectral region, which is also one of the challenges to be addressed in future deep ultraviolet SHG switching materials.

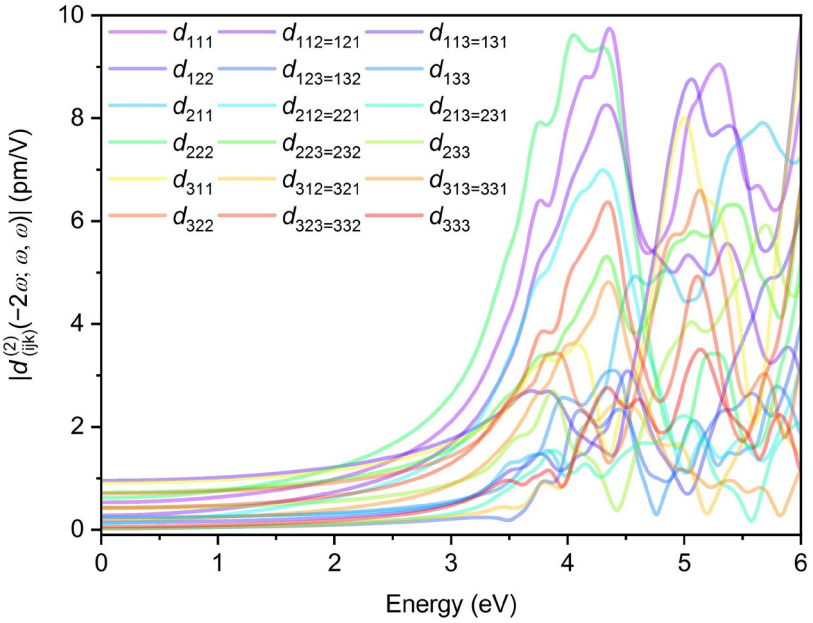

Figure S8. Calculated frequency dependent NLO coefficients of RHSO-LTP.

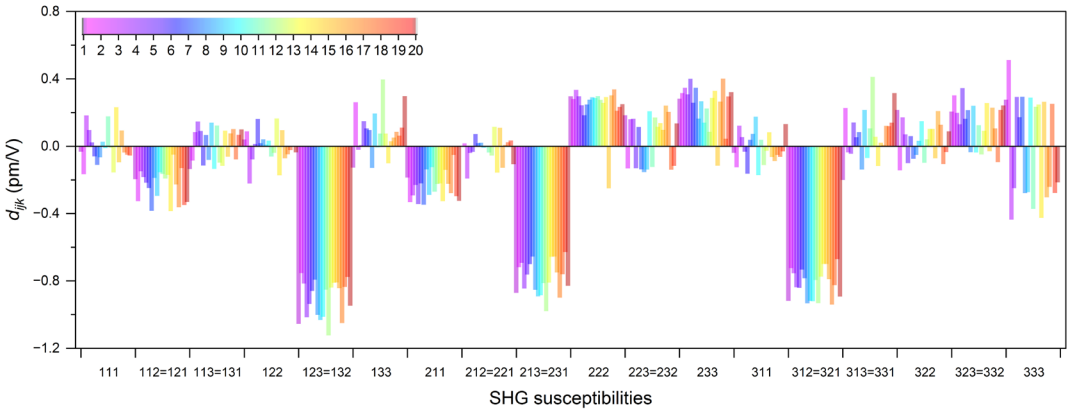

Figure S9. The calculated SHG susceptibilities d_{ijk} at an incident wavelength of 1064 nm, based on the 20 typical *ab initio* molecular dynamic simulated configurations of RHSO at 388 K.

REFERENCES

(1) Dolomanov, O. V.; Bourhis, L. J.; Gildea, R. J.; Howard, J. A. K.; Puschmann, H. *OLEX2*: A Complete Structure Solution, Refinement and Analysis Program. *J. Appl. Crystallogr.* **2009**, *42*, 339–341.

(2) Sheldrick, G. M. *SHELXT*−Integrated Space-Group and Crystal-Structure Determination. *Acta Crystallogr., Sect. A: Found. Adv.* **2015**, *71*, 3–8.

(3) Sheldrick, G. M. Crystal Structure Refinement with *SHELXL*. *Acta Crystallogr., Sect. C: Struct. Chem.* **2015**, *71*, 3–8.

(4) Kurtz, S. K.; Perry, T. T. A Powder Technique for the Evaluation of Nonlinear Optical Materials. *J. Appl. Phys.* **1968**, *39*, 3798–3813.

(5) Clark, S. J.; Segall, M. D.; Pickard, C. J.; Hasnip, P. J.; Probert, M. I. J.; Refson, K.; Payne, M. C. First Principles Methods Using CASTEP. *Z. Kristallogr. - Cryst. Mater.* **2005**, *220*, 567–570.

(6) Perdew, J. P.; Burke, K.; Ernzerhof, M. Generalized Gradient Approximation Made Simple. *Phys. Rev. Lett.* **1996**, *77*, 3865.

(7) Aversa, C.; Sipe, J. E. Nonlinear Optical Susceptibilities of Semiconductors: Results With a Length-Gauge Analysis. *Phys. Rev. B: Condens. Matter Mater. Phys.* **1995**, *52*, 14636–14645.

(8) Nastos, F.; Olejnik, B.; Schwarz, K.; Sipe, J. E. Scissors Implementation Within Length-Gauge Formulations of the Frequency-Dependent Nonlinear Optical Response of Semiconductors. *Phys. Rev. B: Condens. Matter Mater. Phys.* **2005**, *72*, 045223.

(9) Chen, C.; Lin, Z.; Wang, Z. The development of new boratebased UV nonlinear optical crystals. *Appl. Phys. B: Lasers Opt.* **2005**, *80*, 1–25.

(10) Perdew, J. P.; Wang, Y. Accurate and simple analytic representation of the electron-gas correlation energy. *Phys. Rev. B: Condens. Matter Mater. Phys.* **1992**, *45*, 13244–13249.

(11) Heyd, J.; Scuseria, G. E.; Ernzerhof, M. Hybrid functionals based on a screened coulomb potential. *J. Chem. Phys.* **2003**, *118*, 8207–8215.

(12) Krukau, A. V.; Vydrov, O. A.; Izmaylov, A. F.; Scuseria, G. E. Influence of the exchange screening parameter on the performance of screened hybrid functionals. *J. Chem. Phys.* **2006**, *125*, 224106.

(13) Car, R.; Parrinello, M. Unified approach for molecular dynamics and density-functional theory. *Phys. Rev. Lett.*, **1985**, *55*, 2471–2474.

(14) Grimme, S. Semiempirical GGA-type density functional constructed with a long-range dispersion correction. *J. Comput. Chem.*, **2006**, *27*, 1787–1799.

(15) Martyna, G. J.; Klein, M. L.; Tuckerman, M. Nose–Hoover chains: The canonical ensemble via continuous dynamics. *J. Chem. Phys.*, **1992**, *97*, 2635–2643.

(16) Vanderbilt, D. Soft self-consistent pseudopotentials in a generalized eigenvalue formalism *Phys. Rev. B*, **1990**, *41*, 7892–7895.